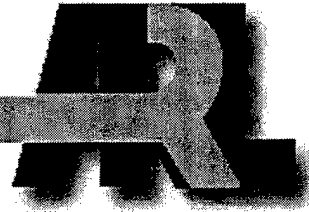


ARMY RESEARCH LABORATORY



Computational Fluid Dynamics Modeling of Submunition Separation From Missile

Harris L. Edge
Jubaraj Sahu
Karen R. Heavey

ARL-TR-1981

MAY 1999

19990618 190

DTIC QUALITY INSPECTED 4

Approved for public release; distribution is unlimited.

The findings in this report are not to be construed as an official Department of the Army position unless so designated by other authorized documents.

Citation of manufacturer's or trade names does not constitute an official endorsement or approval of the use thereof.

Destroy this report when it is no longer needed. Do not return it to the originator.

Army Research Laboratory

Aberdeen Proving Ground, MD 21005-5066

ARL-TR-1981

May 1999

Computational Fluid Dynamics Modeling of Submunition Separation From Missile

Harris L. Edge
Jubaraj Sahu
Karen R. Heavey
Weapons & Materials Research Directorate

Approved for public release; distribution is unlimited.

Abstract

Computational fluid dynamics calculations have been performed for a multi-body system consisting of a main missile and a number of submunitions. Numerical flow field computations have been made for various orientations and locations of submunitions using an unsteady, zonal Navier-Stokes code and the chimera composite grid discretization technique at low supersonic speeds and 0° angle of attack. Steady state numerical results have been obtained and compared for cases modeling six submunitions in pitch-plane symmetry and ten submunitions for which symmetry could not be exploited. Computed results show the details of the expected flow field features including the shock interactions. Computed results are compared with limited experimental data obtained for the same configuration and conditions and are generally found to be in good agreement with the data. The results help to quantify changes in the aerodynamic forces and moments, which are attributable to changes in position of the submunitions relative to one another.

ACKNOWLEDGMENTS

The authors would like to thank the High Performance Computing Center at the Tank-Automotive Command Research, Development, and Engineering Center, Warren, Michigan, and the U.S. Army Research Laboratory Major Shared Research Center at Aberdeen Proving Ground, Maryland, for the use of their computing resources.

INTENTIONALLY LEFT BLANK

TABLE OF CONTENTS

	<u>Page</u>
LIST OF FIGURES	vii
LIST OF TABLES	ix
1. INTRODUCTION	1
2. SOLUTION TECHNIQUE	2
2.1 Governing Equations	2
2.2 Numerical Algorithm	2
2.3 Chimera Scheme	3
3. MULTI-BODY PROBLEM DESCRIPTION	4
4. MODEL GEOMETRY AND GRIDS	5
5. BOUNDARY CONDITIONS	7
6. RESULTS	8
7. CONCLUDING REMARKS	16
REFERENCES	19
DISTRIBUTION LIST	21
REPORT DOCUMENTATION PAGE	25

INTENTIONALLY LEFT BLANK

LIST OF FIGURES

<u>Figure</u>	<u>Page</u>
1. Diagram of Multi-body System	1
2. Inter-grid Communications	4
3. Grids for the BAT Submunition Being Dispensed From TACMS	5
4. Computational Grid for a Submunition	6
5. Computational Grid for the Missile	6
6. Circumferential Cross-sectional Grid	6
7. Mach Contours for the Symmetrical Dispensation Case	9
8. Mach Contours at $X/D = 2.5$ Calibers	9
9. Mach Contours at $X/D = 3.2$ Calibers	9
10. Force and Moment Coefficients	10
11. Diagram of the TACMS and BATs With Fast Mode BAT Shaded	10
12. Configuration A and B Submunition Location	12
13. Normalized Surface Pressure Contours for TACMS and Submunitions in Configuration A	13
14. Normalized Surface Pressure Contours for TACMS and Submunitions in Configuration B	13
15. Locations Where Experimental Data Were Collected	14
16. Pressure Coefficient Versus BAT Length for BAT Surface Facing TACMS	14
17. Pressure Coefficient Versus BAT Length for BAT Surface Facing Away From TACMS	15
18. Force and Moment Coefficients for Configuration A	15
19. Drag Coefficients for Configuration A	16

INTENTIONALLY LEFT BLANK

LIST OF TABLES

<u>Table</u>		<u>Page</u>
1.	Force and Moment Coefficients for Symmetrical Dispensation	11
2.	Force and Moment Coefficients for Fast Mode Dispensation	11

INTENTIONALLY LEFT BLANK

COMPUTATIONAL FLUID DYNAMICS MODELING OF SUBMUNITION SEPARATION FROM MISSILE

1. INTRODUCTION

Aerodynamic forces and moments are critical design parameters used in the design of shell and bodies flying in relative motion to each other. The advancement of computational fluid dynamics (CFD) has had a major impact on projectile design and development.[1-4] Improved computer technology and state-of-the-art numerical procedures enable solutions to complex, three-dimensional (3-D) problems associated with projectile and missile aerodynamics. The research effort has focused on the development and application of a versatile overset grid numerical technique to solve multi-body aerodynamic problems. This numerical capability has been used successfully to determine the aerodynamics on a multi-body problem of brilliant anti-armor (BAT) submunition dispersal from the Army tactical missile system (TACMS). Figure 1 shows this missile and multiple submunition system.

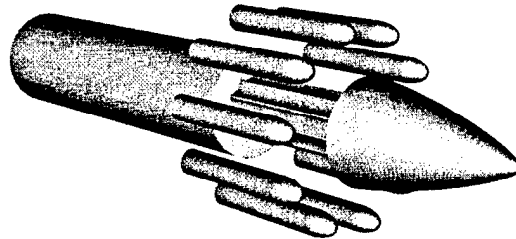


Figure 1. Diagram of Multi-body System.

The complexity and uniqueness of this type of multi-body problem result from the aerodynamic interference of the individual components, which include 3-D shock-shock interactions, shock-boundary layer interactions, and highly viscous-dominated separated flow regions. The overset grid technique, which is ideally suited to this problem, involves generating numerical grids about each body component and then oversetting them onto a base grid to form the complete model. With this composite overset grid approach, it is possible to determine the 3-D interacting flow field of the multi-body system and the associated aerodynamic forces and moments at different positions and orientations without the need for costly regridding. The solution procedure of the developed technique is to compute the interference flow field at multiple locations until final converged solutions are obtained and then to integrate the pressure and viscous forces to obtain the total

forces and moments. The complex physics and fluid dynamics structure of the 3-D aerodynamic interference for this multi-body problem have been identified.

A description of the computational algorithm and the chimera technique follows. The next section describes the model geometry and various computational grids used in the numerical computations. Results are shown for multiple BAT submunitions at low supersonic speeds. In one set of computations, the effects of a single submunition dispensing too quickly are investigated. Another set of computations is designed to investigate the flow field for the nonsymmetrical dispensation of submunitions near and far from the TACMS missile bay.

2. SOLUTION TECHNIQUE

2.1 Governing Equations

The complete set of 3-D, time-dependent, generalized geometry, Reynolds-averaged, thin layer Navier-Stokes equations is solved numerically to obtain a solution to this problem and can be written in general spatial coordinates ξ , η , and ζ as follows [5]:

$$\partial_\tau \hat{q} + \partial_\xi \hat{F} + \partial_\eta \hat{G} + \partial_\zeta \hat{H} = R_e^{-1} \partial_\zeta \hat{S}. \quad (1)$$

In Equation 1, \hat{q} contains the dependent variables: density, three velocity components, and energy. The thin layer approximation is used here, and the viscous terms involving velocity gradients in both the longitudinal and circumferential directions are neglected. The viscous terms are retained in the normal direction, ζ , and are collected into the vector \hat{S} . These viscous terms are used everywhere. In the wake or the base region, similar viscous terms [1] are also added in the stream-wise direction, ξ . An implicit, approximately factored scheme is used to solve these equations.

2.2 Numerical Algorithm

The implicit, approximately factored scheme for the thin layer Navier-Stokes equations using central differencing in the η and ζ directions and an upwind scheme in ξ is written in the following form [6]:

$$\begin{aligned} & \left[I + i_b h \delta_\xi^b (\hat{A}^+)^n + i_b h \delta_\zeta \hat{C}^n - i_b h R_e^{-1} \bar{\delta}_\zeta J^{-1} \hat{M}^n J i_b D_i |_\zeta \right] x \\ & \left[I + i_b h \delta_\xi^f (\hat{A}^-)^n + i_b h \delta_\eta \hat{B}^n - i_b D_i |_\eta \right] \Delta \hat{Q}^n = -i_b \Delta t \\ & \left\{ \delta_\xi^b \left[(\hat{F}^+)^n - \hat{F}_\infty^+ \right] + \delta_\xi^f \left[(\hat{F}^-)^n - \hat{F}_\infty^- \right] + \delta_\eta \left[\hat{G}^n - \hat{G}_\infty \right] + \delta_\zeta \left[\hat{H}^n - \hat{H}_\infty \right] - R_e^{-1} \bar{\delta}_\zeta \left[\hat{S}^n - \hat{S}_\infty \right] \right\} \\ & \quad - i_b D_e \left[\hat{Q}^n - \hat{Q}_\infty \right], \end{aligned} \quad (2)$$

in which $h = \Delta t$ or $(\Delta t)/2$ and the free stream base solution is used. Here, δ is typically a three-point second order accurate central difference operator, $\bar{\delta}$ is a midpoint operator used with the viscous terms, and the operators δ_{ξ}^b and δ_{ξ}^f are backward and forward three-point difference operators. The flux \hat{F} has been eigensplit, and the matrices \hat{A} , \hat{B} , \hat{C} , and \hat{M} result from local linearization of the fluxes about the previous time level. Here, J denotes the Jacobian of the coordinate transformation. Dissipation operators D_e and D_i are used in the central space differencing directions.

2.3 Chimera Scheme

The chimera overset grid technique [7–9], which is ideally suited to multi-body problems, involves generating independent grids about each body and then oversetting them onto a base grid to form the complete model. This procedure reduces a complex multi-body problem into a number of simpler sub-problems. An advantage of the overset grid technique is that it allows computational grids to be obtained for each body component separately and thus makes the grid generation process easier. Because each component grid is generated independently, portions of one grid may lie within a solid boundary contained within another grid. Such points lie outside the computational domain and are excluded from the solution process. Equation 2 has been modified for chimera overset grids by the introduction of the flag i_b to achieve just that. This i_b array accommodates the possibility of having arbitrary holes in the grid. The i_b array is defined so that $i_b = 1$ at normal grid points and $i_b = 0$ at hole points. Thus, when $i_b = 1$, Equation 2 becomes the standard scheme, but when $i_b = 0$, the algorithm reduces to $\Delta \hat{Q}^n = 0$ or $\hat{Q}^{n+1} = \hat{Q}^n$, leaving \hat{Q} unchanged at hole points. The set of grid points that forms the border between the hole points and the normal field points is called inter-grid boundary points. These points are updated by interpolating the solution from the overset grid that created the hole. Values of the i_b array and the interpolation coefficients needed for this update are provided by a separate algorithm [7].

Figure 2 shows an example where the parent missile grid is a major grid and the BAT submunition grid is a minor grid. The submunition grid is completely overlapped by the missile grid, and thus its outer boundary can obtain information by interpolation from the missile grid. Similar data transfer or communication is needed from the submunition grid to the missile grid. However, a natural outer boundary that overlaps the submunition grid does not exist for the missile grid. The overset grid technique creates an artificial boundary or a hole boundary within the missile grid that provides the required path for information transfer from the submunition grid to the missile grid. The resulting hole region is excluded from the flow field solution in the missile grid.

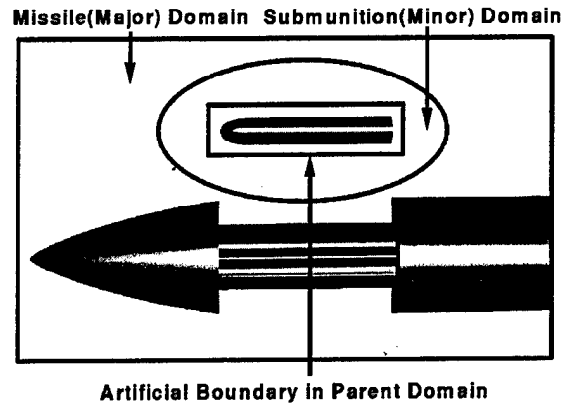


Figure 2. Inter-grid Communications.

3. MULTI-BODY PROBLEM DESCRIPTION

The TACMS-BAT multi-body problem involves the radial dispensing of several BAT submunitions (see Figure 1) at a low supersonic speed and was therefore ideally suited for the numerical capability [11] described earlier. The 3-D radial dispensing of these submunitions depends on the initial ejection velocity. The flow field is complex and involves 3-D shock-boundary layer interactions and TACMS-to-BAT as well as BAT-to-BAT interactions. Detailed experimental or theoretical data were not available to help evaluate the submunition dispensing phenomenon for the entire BAT system, and thus the numerical solution of this problem was initiated. The chimera solution procedure was thus used to determine the aerodynamic interference effects, and CFD was brought into the developmental phase of the BAT program to ensure successful dispensing of the submunitions. Previous CFD work for this application has been documented in references 12, 13, and 14. Reference 13 may be of particular interest to those interested in dynamic CFD modeling because it documents an unsteady viscous CFD computation of symmetrical BAT submunition separation from the TACMS using the chimera technique. This report does not present unsteady results. The computational results reported document steady state CFD computations of the BATs located at differing radii about the TACMS to quantify the effects of asymmetrical BAT dispensation from the TACMS submunition bay.

The missile carries 13 submunitions; the first ten outer BAT submunitions are radially dispensed, and then the three inner BAT submunitions are dispensed from the TACMS. Once released from the missile bay, the self-guided BAT submunitions autonomously navigate over the hostile territory, use their sensors to detect targets, and deliver shaped charged warheads. The concern here is the flight dynamics and aerodynamics of the dispensing phenomenon. Application of the advanced CFD modeling technique to this multi-body dispensing problem was to provide

realistic simulation, detailed understanding of the underlying aerodynamic interference effects, and design information that can lead to successfully dispensing the BAT submunitions from the TACMS.

4. MODEL GEOMETRY AND GRIDS

An advantage of the chimera technique is that it allows computational grids to be obtained for each body component separately and makes the grid generation process easier. Figure 3 shows a computational grid for the complete model, including the missile and the BAT submunitions. Also shown here are the sections of the 3-D BAT computational grids overset onto the missile grid. Figure 4 shows a computational grid for one BAT submunition. As part of the chimera procedure, this BAT grid is partially cut by the missile body itself. Similarly, the presence of the BAT submunition cuts a hole in the missile grid (see Figure 5). The missile grid consists of three zones: one on the nose region ahead of the cavity, one in the cavity itself, and the third one aft of the cavity region. Each of these three zones is a rectangular grid. The grid around the submunition consists of two zones (one for the body and one for the base region) and was obtained using a C-topology and a rectangular topology, respectively. The submunition grids were individually generated and then overset as shown in Figure 3 to form the complete grid system. Figure 6 is a close view of a 36° circumferential segment of a plane cutting through BAT submunitions and the missile bay. The computational grids shown in Figures 4 and 5 correspond to the pitch plane. The missile grid serves as the main background grid for the computations. Figure 4 shows a computational grid for computations with the BAT submunition at a distance of about one diameter away from the center line of symmetry of the missile. For steady state or unsteady dynamic computations, the same submunition grids can be used, and there was no need to regenerate new submunition grids.

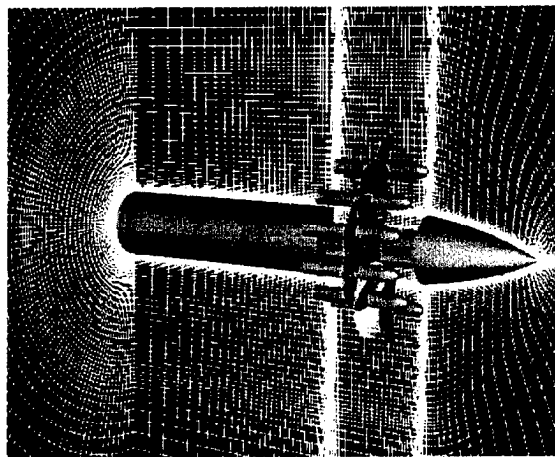


Figure 3. Grids for the BAT Submunition Being Dispensed From TACMS.

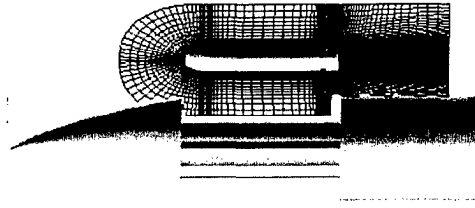


Figure 4. Computational Grid for a Submunition.

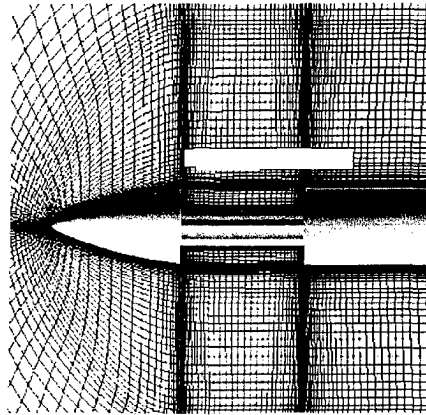


Figure 5. Computational Grid for the Missile.

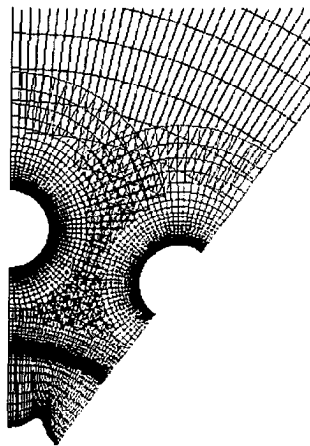


Figure 6. Circumferential Cross-sectional Grid.

For the computations used to examine the effects of a submunition dispensing too quickly, pitch-plane symmetry was assumed, and the total number of computational mesh points was approximately 3.4 million. For cases used to model the effects of asymmetrical dispensation near and far from the TACMS missile bay, no symmetry could be exploited and the computational mesh required approximately 7.4 million points. Note that the grid setup allows computation of the base region flow field of the submunitions. The "stings" required to mount the models in the wind tunnel were not modeled for these cases. Grid points are clustered near the missile and the BAT submunition surfaces to capture the viscous boundary layers. No attempt has been made to adapt the computational grids to gradients in the flow field variables.

The actual cavity surface of the missile bay where the BATs are stored in their original positions was modeled in the CFD computations. Because there are still three bats left in the missile bay once the first ten have been ejected, the missile bay surface model is not axisymmetrical and is an irregular surface. The flow field in the bay is viscously dominated, turbulent, and quite complex, with the BAT located in the near field. It is difficult to accurately determine the interference effects by theoretical or experimental means. This is especially true when the BAT is submerged in the bay. Limited wind tunnel experimental data [15] are available for a reduced scale model for the missile and BAT submunitions. However, such data can suffer from sting effects. Also, since there is a viscously dominated cavity flow, the experiment may not scale to the real flight conditions.

5. BOUNDARY CONDITIONS

Boundary conditions are imposed explicitly. An adiabatic wall boundary condition is used on the body surfaces of the TACMS and BATs. The no-slip condition was specified for each wall surface. For the nose and cylinder portion of the TACMS, and the nose and body of each BAT, pressure at the wall is calculated by solving a combined momentum equation. For the walls of the TACMS bay and at the walls defining the base of each BAT, wall pressure was computed from a zero-order flow field extrapolation. The outer boundary of the TACMS grid was positioned far enough away from the TACMS-BAT configuration to be set at free stream conditions for the computations. Since the free stream is supersonic, a simple flow field extrapolation is used for the down-stream boundary condition of the TACMS grid. The conditions for the outer boundaries of each BAT grid are set by the chimera scheme. A combination of symmetry and extrapolation boundary condition is used on the center line (axis) at the nose of the TACMS and the nose and base of each BAT. For cases when pitch plane symmetry was applicable, a symmetry boundary

condition is imposed at the circumferential edges of the TACMS grid and the circumferential edges of the BAT grids that are positioned on the symmetry plane.

6. RESULTS

Steady state numerical calculations have been performed to numerically simulate the missile and the BAT system. This report presents results for the TACMS-BAT flow field with the BAT located at multiple radial distances from the TACMS axis of symmetry. Computations have been run at $M_\infty = 1.2$. For all computations, the TACMS missile is at 0° angle of attack. Appropriate symmetry is used for the multiple BAT cases. For the multiple BAT cases, the computational domain consists of either a 180° or 360° segment in the circumferential plane. Figure 3 shows the grid configuration for the TACMS-BAT computational domain that models a 180° circumferential flow field. The submunition grids are entirely contained in the background TACMS missile grid.

Computations were performed for the symmetrically dispensed multi-body problem with six BATs at $M_\infty = 1.2$ and $\alpha = 0^\circ$. Two of the six BATs were positioned on the symmetry plane; thus, only 180° of circumferential arc was required to model them. Also, in this case, only half of the actual missile bay was modeled. Figure 7 shows the Mach number contours for this case. Qualitatively, it shows the expected shock structure and the flow field resulting from the submunition interactions. Figures 8 and 9 show the circumferential Mach number contours for the six-BAT case at two longitudinal stations, 2.5 and 3.2 calibers from the nose of the missile. Both locations are in the cavity of the missile; 2.5 calibers correspond to a position approximately at the bay midpoint, while 3.2 calibers is very close to the aft end of the missile bay. These figures show the BAT-to-BAT interactions and the effect of the cavity shape on the solutions. Figure 8 indicates a smaller region of low-speed flow between the cavity surface and the bottom surfaces of the BATs and high-speed flow near the top surfaces of the BATs. At a station down stream in the cavity, Figure 9 shows a large region of the low-speed flow between the BATs and missile cavity surface as well as near and away from the top surfaces of the BATs.

Aerodynamic forces and moments were obtained from the computed solutions. Figure 10 shows normal force coefficient, axial force coefficient, and pitching moment for the submunitions as a function of radius (measured from the center line of symmetry of the missile). These computed force and moment coefficients were compared with the experimental data and are found to be in good agreement with the data. Documentation for the experimental data presented in this report is given in Reference 15. The measured axial force coefficient does not include base drag, and computed axial force coefficient excludes base drag of the submunitions for direct comparison.

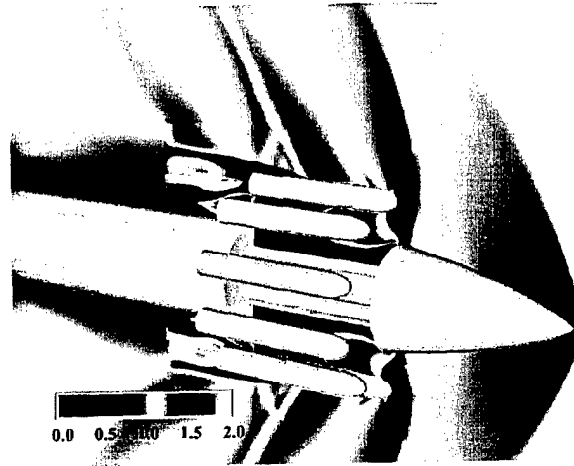


Figure 7. Mach Contours for the Symmetrical Dispensation Case.

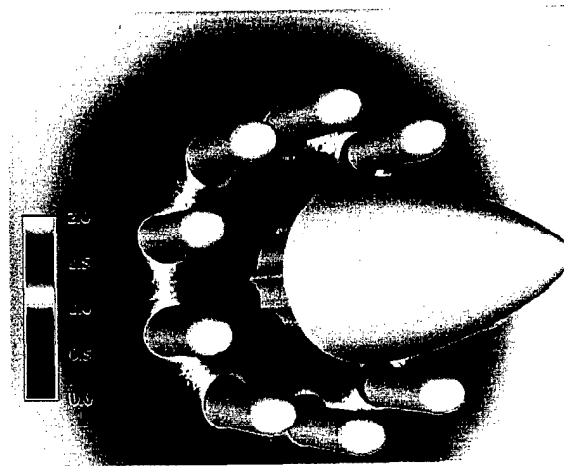


Figure 8. Mach Contours at $X/D = 2.5$ Calibers.

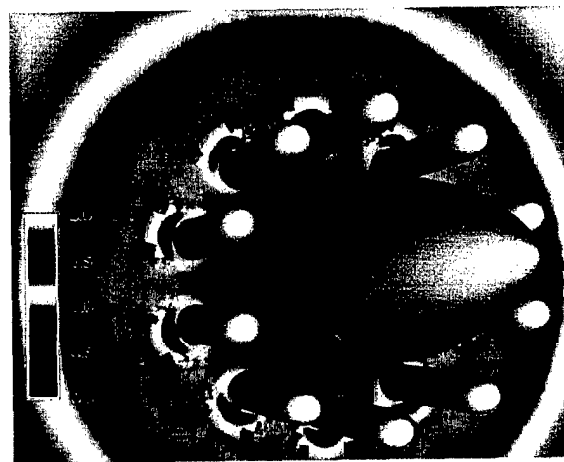


Figure 9. Mach Contours at $X/D = 3.2$ Calibers.

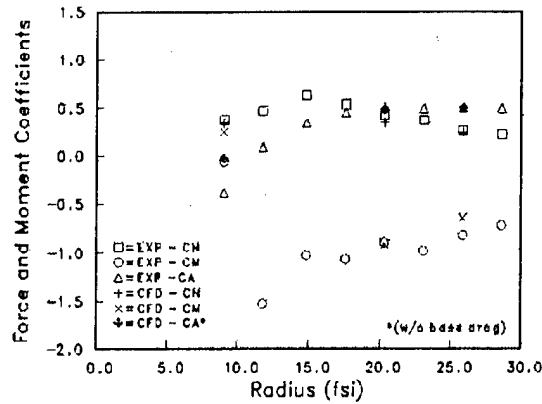


Figure 10. Force and Moment Coefficients.

In order to examine the effect of a single BAT submunition ejecting from the missile bay too quickly, a single submunition was positioned at a radial distance one BAT diameter greater than the rest of the submunitions. This positioning will be referred to as fast mode dispensation. Figure 11 provides a visual reference for the fast mode positioning. The darkly shaded submunition is moved radially outside its symmetrical dispensed position. Tables 1 and 2 show the results for the symmetrical dispensation and fast mode dispensation, respectively. BAT1 represents the uppermost submunition, while BAT6 represents the lowermost submunition. BAT1 is the submunition that is moved by one BAT diameter in the fast mode dispensation position. As can be seen in Tables 1 and 2, the aerodynamic forces and moments on the BATs closest to BAT2 have changed appreciably, as have the forces and moments on BAT1 itself. The influence of the change in BAT1 positioning on BATs 3 through 6 seems to be minimal.

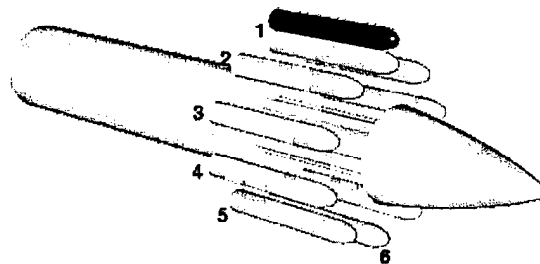


Figure 11. Diagram of the TACMS and BATs With Fast Mode BAT Shaded.

Table 1. Force and Moment Coefficients for Symmetrical Dispensation

BAT NO.	1	2	3	4	5	6
C_Y	0.00000	0.18940	0.43563	0.44073	0.23868	0.00000
C_Z	0.47680	0.44573	0.18260	-0.10102	-0.39834	-0.49379
C_N (radial)	0.47680 0.424*	0.48430	0.47235	0.45216	0.46437	0.49739
C_{my}	-1.74121 -0.896*	-1.41135	-0.37417	0.37417	1.47658	1.67967
C_{mz}	0.00000	0.82260	1.51720	1.52951	0.88127	0.00000
C_A (body)	0.45168 0.500*	0.45791	0.46131	0.46301	0.46857	0.45130
C_A (base)	0.38389	0.42326	0.41731	0.43676	0.43223	0.40712
C_A (total)	0.83557	0.88117	0.87862	0.89977	0.89080	0.85842

* Experimental Data

Table 2. Force and Moment Coefficients for Fast Mode Dispensation

BAT NO.	1**	2	3	4	5	6
C_Y	0.00000	0.25992	0.46471	0.44585	0.23934	0.00000
C_Z	0.28136	0.39588	0.15125	-0.10253	-0.39579	-0.48378
C_N (radial)	0.28136 0.259*	0.47359	0.48871	0.45747	0.46253	0.48378
C_{my}	-1.04292 -0.816*	-1.43104	-0.31263	0.38279	1.45320	1.62551
C_{mz}	0.00000	1.06713	1.64028	1.54017	0.86158	0.00000
C_A (body)	0.47623 0.502*	0.46056	0.46141	0.46244	0.45820	0.45055
C_A (base)	0.26682	0.42534	0.41439	0.42827	0.43620	0.40296
C_A (total)	0.74305	0.88589	0.87579	0.89071	0.89439	0.85351

* Experimental Data ** Radial offset is 25.85 fsi

For another set of runs, the position of the submunitions was set in order to evaluate flow field correction factors for nonsymmetrical dispensation at a distance near and far from the bay. The flow field correction factors are used in six-degree-of-freedom simulations of BAT dispensation for differing conditions. CFD computations were made for two configurations: Configuration A, which places the submunitions relatively close to the missile bay, and Configuration B, which places them farther away from the turbulence generated by the missile bay. For both Configurations A and B, there is equidistant circumferential spacing for each submunition except one, which has a 5° offset. The submunition with the circumferential offset is located at approximately the 11 o'clock position. Figure 12 provides a visual reference for the submunition positions for Configurations A and B.

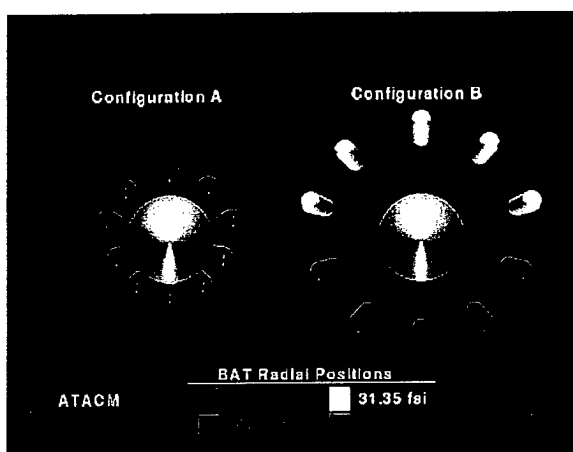


Figure 12. Configuration A and B Submunition Location.

Surface pressure contours are shown for Configuration A in Figure 13 and for Configuration B in Figure 14. The surface pressures on the Configuration A submunitions reveal much stronger pressure gradients than on the submunitions in Configuration B. Also, surface pressure contours within the TACMS missile bay are somewhat different between Configurations A and B. The stronger pressure gradients on the Configuration A submunitions, which are much closer to the TACMS missile bay, are indicative of the higher pitching moments generated, which tend to push the nose of the BAT submunitions radially inward toward the TACMS missile bay. Since the computations include multiple BAT submunitions, BAT-to-BAT interactions are included. These interactions are critical and have a strong effect on the aerodynamic forces and moments. The normal force and pitching moment coefficients vary between the submunitions, indicating the asymmetrical nature of the interacting flow field.

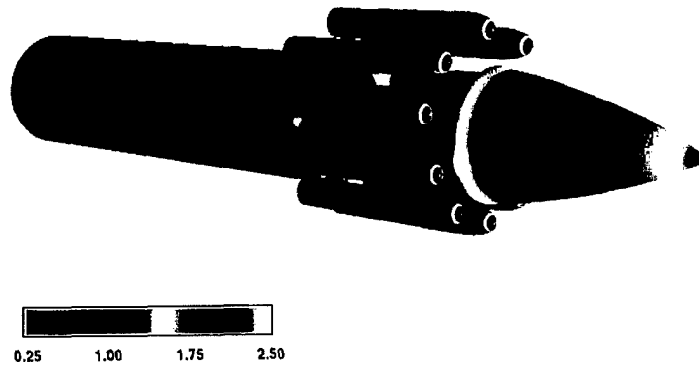


Figure 13. Normalized Surface Pressure Contours for TACMS and Submunitions in Configuration A.

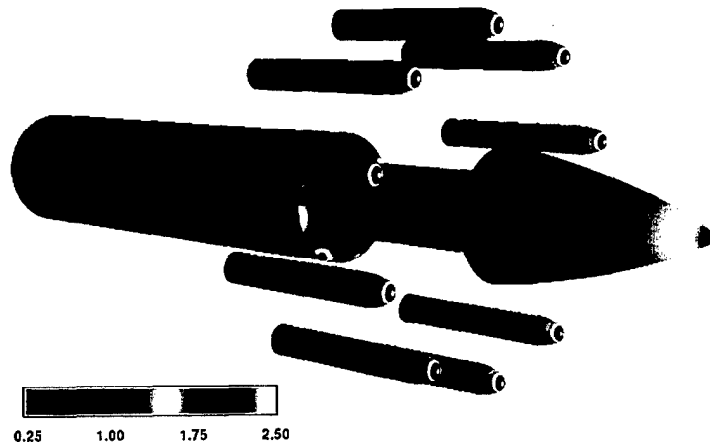


Figure 14. Normalized Surface Pressure Contours for TACMS and Submunitions in Configuration B.

Some experimental data [15] were available for comparisons with the computational results of Configuration A. Figure 15 provides a visual reference for location of the BATs that were the source of the experimental data. A BAT at approximately the 5 o'clock position was equipped to record pressure data. Pressure data were collected on the side of the BAT closest to the TACMS and the side facing away from the TACMS. On either side of the BAT, pressure data were taken at five positions. Unfortunately, the pressure data obtained from the experiment on the side of the BAT facing the TACMS do not appear to be accurate. However, the pressure coefficient data

computed from the CFD solution on the side of the BAT facing the TACMS are plotted in Figure 16. Figure 17 shows a comparison between the pressure coefficient obtained from experimental and CFD-calculated data on the side of the BAT facing away from the TACMS. Both Figures 16 and 17 show the pressure coefficient as a function of the length of the BAT body where $X/L = 0$ corresponds to the BAT nose and $X/L = 1$ corresponds to the end of the BAT body. Figure 17 shows that the pressure coefficient computed from the CFD solution is in very good agreement with experimental data. The CFD-computed data plotted in Figures 16 and 17 provide an interesting comparison that demonstrates the asymmetry of the flow field about the BAT and the strong influence of the TACMS proximity to the BAT. Although the comparison between the experimentally obtained and CFD-computed pressure coefficient is quite good, the comparisons between experimentally obtained and CFD computed force and moments indicate that some flow field characteristics may not be captured accurately by the CFD solution.

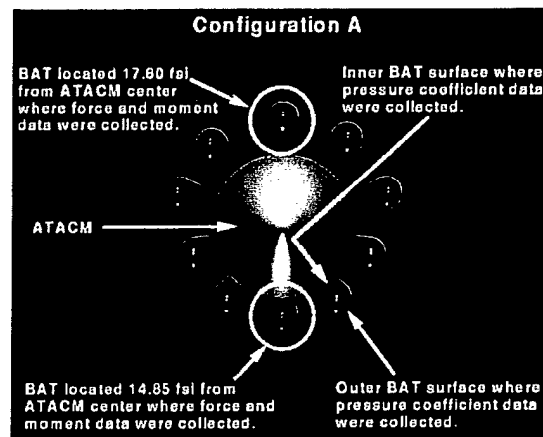


Figure 15. Locations Where Experimental Data Were Collected.

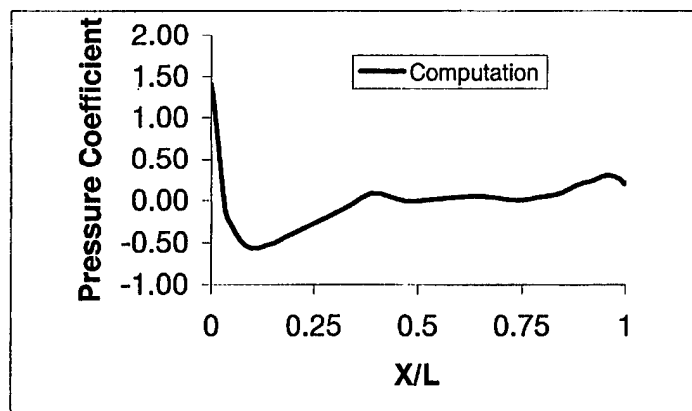


Figure 16. Pressure Coefficient Versus BAT Length for BAT Surface Facing TACMS.

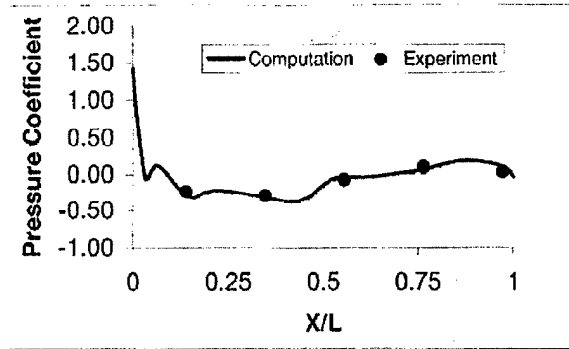


Figure 17. Pressure Coefficient Versus BAT Length for BAT Surface Facing Away From TACMS.

Force and moment data were collected from the BATs located at the 12 o'clock and 6 o'clock positions. The BAT at the 12 o'clock position has a radial distance from the TACMS center of 17.60 full scale inches (fsi). The BAT at the 6 o'clock position has a radial distance from the TACMS center of 14.85 fsi. Figure 18 shows both the experimental data and the data computed from the CFD flow field solution. The data in Figure 18 indicate that the CFD-computed data match the experimental data of the BAT 17.60 fsi from the TACMS center more closely than the experimental and computed data of the BAT 14.85 fsi from the TACMS center. The data for the normal force, CN, are in good agreement for the BAT 17.60 fsi from the TACMS center. The side force, CY, data appear to be the same for the CFD-computed side force and the experimental side force. This is somewhat misleading because the magnitude of the side force is much smaller than the normal force and pitching moment, Cmz (coefficient of moment about the Z axis). The relatively small side force is a good indication that the BATs are not likely to move closer together when being ejected from the TACMS bay at 0° angle of attack. The difference between the pitching moment for experimental data and CFD-computed data is less for the BAT farthest from the TACMS. This seems to indicate increased difficulty in computing the flow field for the TACMS-BAT multi-body problem accurately when the BATs are almost in the TACMS bay.

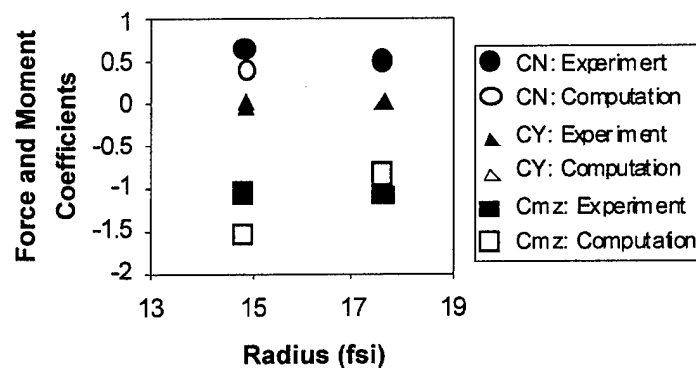


Figure 18. Force and Moment Coefficients for Configuration A.

The drag coefficient computed from the CFD solutions compares very well with the measured drag coefficient. Figure 19 shows a plot for the drag coefficient of the same BATs that were instrumented to obtain the force and moment data displayed in Figure 18. In the experiment, each BAT was mounted on a sting. The stings were not modeled in the CFD computation. The total drag coefficient was obtained from a force measurement of the BAT with sting. The experimental value of the BAT forebody drag was estimated by taking a pressure measurement near the BAT base and using it to estimate the base drag component of the total drag coefficient. The base drag component was then subtracted from the total drag to obtain the forebody drag. An interesting note is the increase in drag with the increased distance of the BAT from the TACMS center.

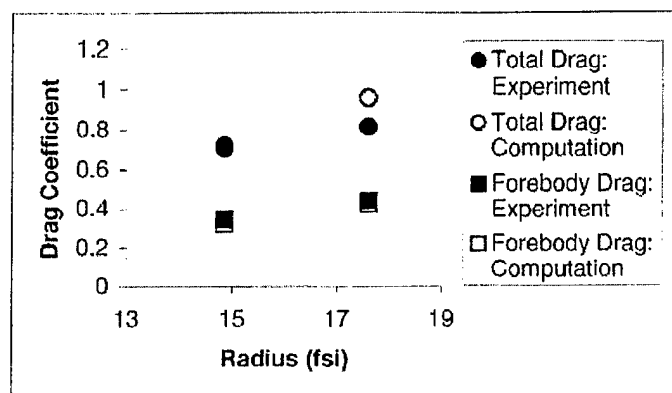


Figure 19. Drag Coefficients for Configuration A.

7. CONCLUDING REMARKS

A computational study was undertaken to compute the 3-D flow fields for a multi-body system consisting of a missile and multiple BAT submunitions. Flow computations were performed at low supersonic speeds ($M_\infty = 1.2$) and $\alpha = 0^\circ$ using a 3-D unsteady Navier-Stokes code and chimera composite grid discretization technique. Overset body-conforming grids were used to individually model the missile and the BAT submunitions. Computed results have been obtained for different radial locations of the BAT submunitions in an effort to gain additional data and understanding of the consequences of an asymmetrical dispensation of ten BATs from the TACMS submunition bay. Computed pressure and Mach contours show the details of the 3-D aerodynamic interference flow field for the missile and the submunitions. The computed flow field includes both the missile-to-BAT as well as BAT-to-BAT interactions, and the presence of these interactions is quite evident in their effect on the computed pressure coefficients, forces, and moments. The CFD-obtained pressure coefficient data compared very well with the pressure coefficient obtained from the experimental data. Computed forces and moments have

been compared with the experimental results for the same configuration and conditions and are generally found to be in good agreement with the data. Future study may include modeling of asymmetrical dynamic submunition dispersal, which will require full 3-D computations and large computing resources.

This work represents the application of a chimera overlapping grids approach for accurate numerical calculation of aerodynamics involving multiple bodies. The predictive numerical capability has been used to provide the development community numerical data and basic flow field design information to more effectively guide the design of a multi-body missile configuration. It allows accurate and realistic numerical prediction of interference effects and aerodynamics required for the improved design and modification of current and future multi-body missile and projectile configurations.

INTENTIONALLY LEFT BLANK

REFERENCES

1. Sahu, J., "Numerical Simulations of Transonic Flows." International Journal for Numerical Methods in Fluids, vol. 10, no. 8, pp. 855-873, 1990.
2. Ferry, E. N., J. Sahu, and K. R. Heavey, "Navier-Stokes Computations of Sabot Discard using Chimera Scheme." Proceedings of the 16th International Symposium on Ballistics, September 1996.
3. Sahu, J., K. R. Heavey, and E. N. Ferry, "Computational Fluid Dynamics for Multiple Projectile Configurations." Proceedings of the 3rd Overset Composite Grid and Solution Technology Symposium, Los Alamos, NM, October 1996.
4. Sahu, J., K. R. Heavey, and C. J. Nietubicz, "Time-Dependent Navier-Stokes Computations for Submunitions in Relative Motion." Proceedings of the 6th International Symposium on Computational Fluid Dynamics, Lake Tahoe, NV, September 1995.
5. Pulliam, T. H., and J. L. Steger, "On Implicit Finite-Difference Simulations of Three-Dimensional Flow," AIAA Journal, vol. 18, no. 2, pp. 159-167, February 1982.
6. Steger, J. L., S. X. Ying, and L. B. Schiff, "A Partially Flux-Split Algorithm for Numerical Simulation of Compressible Inviscid and Viscous Flows." Proceedings of the Workshop on CFD, Institute of Nonlinear Sciences, University of California, Davis, CA, 1986.
7. Steger, J. L., F. C. Dougherty, and J. A. Benek, "A Chimera Grid Scheme," Advances in Grid Generation, edited by K. N. Ghia and U. Ghia, ASME FED-5, June 1983.
8. Benek, J. A., T. L. Donegan, and N. E. Suhs, "Extended Chimera Grid Embedding Scheme With Application to Viscous Flows." AIAA Paper No. 87-1126-CP, 1987.
9. Meakin, R. L., "Computations of the Unsteady Flow About a Generic Wing/Pylon/Finned-Store Configuration." AIAA 92-4568-CP, August 1992.
10. Meakin, R. L., "A New Method for Establishing Inter-Grid Communication Among Systems of Overset Grids," AIAA 10th Computational Fluid Dynamics Conference, AIAA Paper No. 91-1586, June 1991.
11. Sahu, J., and C. J. Nietubicz, "Application of Chimera Technique to Projectiles in Relative Motion." ARL-TR-590, U.S. Army Research Laboratory, Aberdeen Proving Ground, MD, October 1994 (also see AIAA Journal of Spacecraft and Rockets, vol. 32, no. 5, September-October 1995).
12. Wooden, P. A., W. B. Brooks, and J. Sahu, "Calibrating CFD Predictions For Use In Multiple Store Separation Analysis," AIAA Paper No. 98-0754, January 1998.

13. Sahu, J., H. L. Edge, K. R. Heavey, and E. Ferry, "Computational Fluid Dynamics Modeling of Multibody Missile Aerodynamic Interference," Proceedings of the NATO RTO AVT Symposium on Missile Aerodynamics, Sorrento Italy, May 1998.
14. Wooden, P. A., E. R. McQuillen, and W. B. Brooks, "Evaluation of a Simplified Multiple Store Interference Model," AIAA Paper No. 98-2800, June 1998.
15. Lee, P. J., "Analysis Report of Army TACMS Block II Captive Airloads Wind Tunnel Data from HSWT Test 1218," 3-18400/6R-050, Lockheed Martin Vought Systems, Dallas, TX, November 1996.

<u>NO. OF COPIES</u>	<u>ORGANIZATION</u>
2	ADMINISTRATOR DEFENSE TECHNICAL INFO CENTER ATTN DTIC OCP 8725 JOHN J KINGMAN RD STE 0944 FT BELVOIR VA 22060-6218
1	DIRECTOR US ARMY RESEARCH LABORATORY ATTN AMSRL CS AL TA REC MGMT 2800 POWDER MILL RD ADELPHI MD 20783-1197
1	DIRECTOR US ARMY RESEARCH LABORATORY ATTN AMSRL CI LL TECH LIB 2800 POWDER MILL RD ADELPHI MD 207830-1197
1	DIRECTOR US ARMY RESEARCH LABORATORY ATTN AMSRL DD J J ROCCHIO 2800 POWDER MILL RD ADELPHI MD 20783-1197
7	CDR US ARMY ARDEC ATTN AMSTE AET A R DEKLEINE C NG R BOTTICELLI H HUDGINS J GRAU S KAHN W KOENIG PICATINNY ARSENAL NJ 07806-5001
1	CDR US ARMY ARDEC ATTN AMSTE CCH V PAUL VALENTI PICATINNY ARSENAL NJ 07806-5001
1	CDR US ARMY ARDEC ATTN SFAE FAS SD MIKE DEVINE PICATINNY ARSENAL NJ 07806-5001
2	USAF WRIGHT AERONAUTICAL LABS ATTN AFWAL FIMG DR J SHANG MR N E SCAGGS WPAFB OH 45433-6553
3	AIR FORCE ARMAMENT LAB ATTN AFATL/FXA STEPHEN C KORN BRUCE SIMPSON DAVE BELK EGLIN AIR FORCE BASE FL 32542-5434
1	CDR NSWC CODE B40 DR W YANTA DAHLGREN VA 22448-5100

<u>NO. OF COPIES</u>	<u>ORGANIZATION</u>
1	CDR NSWC CODE 420 DR A WARDLAW INDIAN HEAD MD 20640-5035
1	CDR NSWC ATTN DR F MOORE DAHLGREN VA 22448
1	NAVAL AIR WARFARE CENTER ATTN DAVID FINDLAY MS 3 BLDG 2187 PATUXENT RIVER MD 20670
4	DIR NASA LANGLEY RESEARCH CENTER ATTN TECH LIBRARY MR D M BUSHNELL DR M J HEMSCH DR J SOUTH LANGLEY STATION HAMPTON VA 23665
2	ARPA ATTN DR P KEMMEY DR JAMES RICHARDSON 3701 NORTH FAIRFAX DR ARLINGTON VA 22203-1714
7	DIR NASA AMES RESEARCH CENTER MS 227 8 L SCHIFF MS 258 1 T HOLST MS 258 1 D CHAUSSEE MS 258 1 M RAI MS 258 1 P KUTLER MS 258 1 P BUNING MS 258 1 B MEAKIN MOFFETT FIELD CA 94035
2	USMA DEPT OF MECHANICS ATTN LTC ANDREW L DULL M COSTELLO WEST POINT NY 10996
2	UNIV OF CALIFORNIA DAVIS DEPT OF MECHANICAL ENGRG ATTN PROF H A DWYER PROF M HAFEZ DAVIS CA 95616

<u>NO. OF COPIES</u>	<u>ORGANIZATION</u>	<u>NO. OF COPIES</u>	<u>ORGANIZATION</u>
1	AEROJET ELECTRONICS PLANT ATTN DANIEL W PILLASCH B170 DEPT 5311 PO BOX 296 1100 WEST HOLLYVALE STREET AZUSA CA 91702	1	UNIVERSITY OF MARYLAND DEPT OF AEROSPACE ENGRG ATTN DR J D ANDERSON JR COLLEGE PARK MD 20742
1	MIT TECH LIBRARY 77 MASSACHUSETTS AVE CAMBRIDGE MA 02139	1	UNIVERSITY OF NOTRE DAME DEPT OF AERONAUTICAL & MECH ENGRG ATTN PROF T J MUELLER NOTRE DAME IN 46556
1	GRUMANN AEROSPACE CORP AEROPHYSICS RESEARCH DEPT ATTN DR R E MELNIK BETHPAGE NY 11714	1	UNIVERSITY OF TEXAS DEPT OF AEROSPACE ENGRG MECH ATTN DR D S DOLLING AUSTIN TX 78712-1055
2	MICRO CRAFT INC ATTN DR JOHN BENEK NORMAN SUHS 207 BIG SPRINGS AVE TULLAHOMA TN 37388-0370	1	UNIVERSITY OF DELAWARE DEPT OF MECHANICAL ENGRG ATTN DR JOHN MEAKIN NEWARK DE 19716
1	LANL ATTN MR BILL HOGAN MS G770 LOS ALAMOS NM 87545	4	COMMANDER USAAMCOM ATTN AMSAM RD SS AT ERIC KREEGER GEORGE LANDINGHAM CLARK D MIKKELSON ED VAUGHN REDSTONE ARSENAL AL 35898-5252
1	METACOMP TECHNOLOGIES INC ATTN S R CHAKRAVARTHY 650 S WESTLAKE BLVD SUITE 200 WESTLAKE VILLAGE CA 91362-3804	4	LOCKHEED MARTIN VOUGHT SYS PO BOX 65003 M/S EM 55 ATTN PERRY WOODEN W B BROOKS JENNIE FOX ED MCQUILLEN DALLAS TX 75265-0003
2	ROCKWELL SCIENCE CENTER ATTN S V RAMAKRISHNAN V V SHANKAR 1049 CAMINO DOS RIOS THOUSAND OAKS CA 91360	1	COMMANDER US ARMY TACOM-ARDEC BLDG 162S ATTN AMCPM DS MO PETER J BURKE PICATINNY ARSENAL NJ 07806-5000
1	ADVANCED TECHNOLOGY CTR ARVIN/CALSPAN AERODYNAMICS RESEARCH DEPT ATTN DR M S HOLDEN PO BOX 400 BUFFALO NY 14225		<u>ABERDEEN PROVING GROUND</u>
1	UNIV OF ILLINOIS AT URBANA CHAMPAIGN DEPT OF MECH & IND ENGINEERING ATTN DR J C DUTTON URBANA IL 61801	2	DIRECTOR US ARMY RESEARCH LABORATORY ATTN AMSRL CI LP (TECH LIB) BLDG 305 APG AA
		2	CDR US ARMY ARDEC FIRING TABLES BRANCH ATTN R LIESKE R EITMILLER F MIRABELLE BLDG 120

<u>NO. OF COPIES</u>	<u>ORGANIZATION</u>	<u>NO. OF COPIES</u>	<u>ORGANIZATION</u>
1	DIR USARL ATTN AMSRL CI C NIETUBICZ BLDG 394	1	DIR USARL ATTN AMSRL WM BF J LACETERA BLDG 120
3	DIR USARL ATTN AMSRL CI H D HISLEY D PRESSEL C ZOLTANI BLDG 394	1	DIR USARL ATTN AMSRL WM TB R LOTTERO BLDG 309
			<u>ABSTRACT ONLY</u>
1	DIR USARL ATTN AMSRL CI H W STUREK BLDG 328	1	DIRECTOR US ARMY RESEARCH LABORATORY ATTN AMSRL CS AL TP TECH PUB BR 2800 POWDER MILL RD ADELPHI MD 20783-1197
2	DIR USARL ATTN AMSRL WM I MAY L JOHNSON BLDG 4600		
2	DIR USARL ATTN AMSRL WM B A W HORST JR W CIEPIELLA BLDG 4600		
1	DIR USARL ATTN AMSRL WM B E M SCHMIDT BLDG 390A		
7	DIR ARL ATTN AMSRL WM BA W D'AMICO F BRANDON T BROWN L BURKE J CONDON B DAVIS M HOLLIS BLDG 4600		
20	DIR USARL ATTN AMSRL WM BC P PLOSTINS M BUNDY G COOPER H EDGE (5 cys) J GARNER B GUIDOS K HEAVEY D LYON A MIKHAIL V OSKAY J SAHU K SOENCKSEN D WEBB P WEINACHT S WILKERSON A ZIELINSKI BLDG 390		
1	DIR USARL ATTN AMSRL WM BD B FORCH BLDG 4600		
2	DIR USARL AMSRL WM BE M NUSCA J DESPIRITO BLDG 390		

INTENTIONALLY LEFT BLANK

